Wave-packet continuum-discretization approach to ion-atom collisions: Nonrearrangement scattering

I. B. Abdurakhmanov, A. S. Kadyrov, and I. Bray

Phys. Rev. A **94**, 022703 — Published 8 August 2016

DOI: 10.1103/PhysRevA.94.022703

Wave-packet continuum-discretisation approach to ion-atom collisions: I. Non-rearrangement scattering

I. B. Abdurakhmanov, A. S. Kadyrov, and I. Bray
Curtin Institute for Computation and department of Physics, Astronomy and Medical Radiation Science, Curtin University, GPO Box U1987, Perth, WA 6845, Australia

A general single-centre close-coupling approach based on a continuum-discretisation procedure is developed to calculate excitation and ionization processes in ion-atom collisions. The continuous spectrum of the target is discretised using stationary wave packets constructed from the Coulomb wave functions, the eigenstates of the target Hamiltonian. Such continuum discretisation allows one to generate pseudostates with arbitrary energies and distribution. These features are ideal for detailed differential ionization studies. The approach starts from the semiclassical three-body Schrödinger equation for the scattering wave function and leads to a set of coupled differential equations for the transition probability amplitudes. To demonstrate its utility the method is applied to calculate collisions of antiprotons with atomic hydrogen. A comprehensive set of benchmark results from integrated to fully differential cross sections for antiproton-impact ionization of hydrogen in the energy range from 1 keV to 1 MeV is provided. Contrary to previous predictions, we find that at low incident energies the singly differential cross section has a maximum away from the zero emission energy. This feature could not be seen without a fine discretisation of the low-energy part of the continuum.

PACS numbers: 34.10.+x, 34.50.Gb, 25.43.+t

I. INTRODUCTION

Ion-atom collisions play an important role in many applications from astrophysics through to cancer therapy [1]. Accurate solution of the ion-atom scattering problem is challenging due to the existence of many reaction channels. At low energies molecular-orbital close-coupling methods are used [2, 3]. At sufficiently high energies perturbative methods [4–7] are accurate. In the intermediate energy region various atomic-orbital close-coupling [8–13], the lattice-based [14–16] and Faddeev [17–21] methods are used. Recently we have developed semiclassical (SC-CCC) [22, 23] and quantum-mechanical (QM-CCC) [24, 25] versions of the convergent close-coupling method. Most of the presently available close-coupling approaches are based on the expansion of the scattering wave function in terms of electronic states of the target. An adequate description of the electronic structure of the target is one of the important requirements for the accurate calculations of the collision cross sections. For instance, if we consider scattering on atomic hydrogen, the negative energy bound states are known exactly and suitable for calculations. However, the true continuum wave functions, which are the exact solutions of the Schrödinger equation for the atomic hydrogen, become problematic in close-coupling calculations since they are not square-integrable. Therefore, in order to account for channels associated with ionization, alternative treatments of the target have been developed like the concept of pseudostates. A suitable choice of the pseudostates can effectively discretize the target continuum making incorporating the continuum into the close-coupling formalism. Indeed, practically all available highly-sophisticated approaches that are valid over a wide energy range are based on expansion of the total scattering wave function using a certain pseudostate basis. The main difference between all these approaches is the way how the continuum is discretised. For instance, Hall *et al.* [26] used Slater orbitals, Pons [27] spherical Bessel functions, Abdurakhmanov *et al.* [28], Igarashi *et al.* [29] and McGovern *et al.* [30] Laguerre functions, Toshima [31] Gaussian-type orbitals, Azuma *et al.* [32] and Sahoo *et al.* [33] B-spline orbitals as basis functions. These basis functions are used to diagonalize the target Hamiltonian which defines the pseudostate wave functions and energies.

The generated discrete basis must meet certain requirements. In particular, the discretisation of the continuum must be sufficiently dense in order to achieve convergent cross sections. As the basis size is increased the negative-energy states converge to the true discrete eigenstates, while the positive-energy states provide an increasingly dense discretization of the continuum. The values of the pseudostate energies depend on the specific choice of basis parameters and in general the energies of the highest lying pseudostates are significantly larger than the values of lower lying pseudostates. One common feature of all of these basis functions is that they produce pseudostates with energies distributed only in a certain way which cannot be changed arbitrarily. This can become an issue if collisions requiring denser discretization at various continuum regions are desired. Also, continuum distributions for different angular momenta produced by the available basis functions are always unaligned which makes calculations of differential ionization cross sections problematic.

In a two-part communication we develop a general close-coupling approach to ion-atom collisions based on a wave-packet continuum-discretisation procedure. The approach allows to accurately calculate all processes tak-

ing place in the collision system. The continuous spectrum of the target is discretised using stationary wave packets constructed from the Coulomb wave functions, the eigenstates of the target Hamiltonian. To this end we utilize special normalized states which we call the wave packets. The wave packets will be constructed based on the idea of eigendifferentials developed long ago by Weyl [34], Wigner and Griffin [35], Bethe [36] and others to treat non-normalizable continuum states (which do not belong to a Hilbert space) in a framework of the standard theory of Hermitian operators in a Hilbert space. The idea has been used successfully in the continuum-discretized coupled-channels approach to nuclear reactions for a few decades [37]. Most recently the close-coupling approach based on the wave packet expansion has been developed by Kukulin and coworkers in the context of the integral-equation formulation of scattering theory [38, 39]. The approach was applied to nuclear collisions and yielded promising results. Schiwietz [40] used single-centre close-coupling approach based on time-dependent wave packets to calculate stopping powers in ion-atom collisions. However, the time-dependent wave packets are not very practical and lead to cumbersome calculations. This could be one of the reasons why the wave-packet continuum discretisation method has not seen further development in atomic physics.

Here we use the stationary wave packets in the framework of our single-center semiclassical convergent close coupling (SC-CCC) approach [22, 41, 42]. The approach starts from the semiclassical three-body Schrödinger equation for the scattering wave function and leads to a set of coupled differential equations for the transition probability amplitudes. The previous implementation was based on the Laguerre pseudostates. Wave-packet continuum discretisation allows one to generate pseudostates with arbitrary energies and distribution. These features are ideal for detailed differential ionization studies. To demonstrate its utility the wave-packet convergent close-coupling (WP-CCC) method is applied to calculate collisions of antiprotons with atomic hydrogen.

Within the energy range of our interest antiproton scattering on atomic hydrogen is the simplest single-center three-body Coulomb problem. It serves as a testing ground for new theoretical approaches under development. The problem has been investigated using the semiclassical close-coupling [26, 27, 29–33, 43, 44] and lattice [45–47] methods, and quantum-mechanical CCC method [28, 48]. The results of the aforementioned theories for the total ionization cross section and other integrated cross sections (where available) are in overall good agreement with each other and the deviation does not exceed 10% at any considered energy. Application to differential ionization cross sections is less certain.

In Sec. II, we give a brief outline of the formalism and describe the procedure for generating the wave packets. Details of the calculations are given in Sec. III and the results are presented in Sec. IV. Finally, in Sec. V we highlight the main findings and draw conclusions from this work. Atomic units are used throughout unless otherwise specified.

II. WAVE-PACKET APPROACH

We treat antiproton-hydrogen scattering within the framework of the one-center semiclassical convergent-close-coupling approach developed previously [22, 42]. The approach follows from the exact three-body formalism, where the total scattering wave function Ψ_i^+ satisfies the full Schrödinger equation

$$(H - E)\Psi_i^+ = 0. \tag{1}$$

The total three-body Hamiltonian operator H is written as

$$H = -\frac{\nabla_{\boldsymbol{R}}^2}{2\mu} - \frac{\nabla_{\boldsymbol{r}}^2}{2} - \frac{1}{r} + \frac{1}{|\boldsymbol{R} - \boldsymbol{r}|} - \frac{1}{R}, \tag{2}$$

where μ is the reduced mass of the projectile-target system, R and r are the positions of the incident antiproton and the orbital electron relative to the nucleus of hydrogen. We assume the target nucleus is located at the origin and the projectile is moving along a classical trajectory $\boldsymbol{R} = \boldsymbol{b} + \boldsymbol{v}t$, where $\boldsymbol{b}$ is the impact parameter and $\boldsymbol{v}$ is the initial velocity of the projectile relative to the target, defined so that $\boldsymbol{b} \cdot \boldsymbol{v} = 0$. Following Bransden and McDowell [49] we separate the total scattering wave function Ψ_i^+ into nuclear and electronic parts according to

$$\Psi_i^+ = e^{i\boldsymbol{q}\boldsymbol{R}}\Psi_{\rm e}, \tag{3}$$

where $\boldsymbol{q}$ is the incident momentum of the projectile relative to the target nucleus. After inserting this into Eq. (1) and using semiclassical approximation we obtain the non-relativistic semiclassical time-dependent Schrödinger equation for the electronic part of the total scattering wave function

$$(H_{\rm t} + V)\Psi_{\rm e}(t, \boldsymbol{r}, \boldsymbol{R}) = i\frac{\partial\Psi_{\rm e}(t, \boldsymbol{r}, \boldsymbol{R})}{\partial t}, \tag{4}$$

where $H_{\rm t}$ is the target Hamiltonian

$$H_{\rm t} = -\nabla_{\boldsymbol{r}}^2/2 - 1/r \tag{5}$$

and

$$V = -1/R + 1/|\boldsymbol{R} - \boldsymbol{r}| \tag{6}$$

is the interaction potential between the projectile and the target constituents. The scattering wave function is expanded in terms of certain basis functions $\psi_\alpha(\boldsymbol{r})$, suitably chosen to represent the full set of target states, as

$$\Psi_{\rm e}(t, \boldsymbol{r}, \boldsymbol{R}) = \sum_{\alpha=1}^{N} a_\alpha(t, \boldsymbol{b})\psi_\alpha(\boldsymbol{r})e^{-i\epsilon_\alpha t}, \tag{7}$$

where N is the number of basis functions and ϵ_α is the energy of the target electronic state α. The latter collectively denotes the full set of quantum numbers in that state. The expansion coefficients $a_\alpha(t, \boldsymbol{b})$ at $t \to +\infty$ represent the transition amplitudes into the various target states.

Substituting this representation of the scattering wave function into the semiclassical Schrödinger equation (4), and using the orthogonality properties of the target wave packets, one obtains the following set of the first-order differential equations for the time-dependent coefficients

$$i\frac{da_\alpha(t,\boldsymbol{b})}{dt} = \sum_{\beta=1}^{N} e^{i(\epsilon_\alpha-\epsilon_\beta)t}\langle\psi_\alpha|V|\psi_\beta\rangle a_\beta(t,\boldsymbol{b}), \quad (8)$$

where $\alpha = 1, 2, \ldots, N$. This system is solved subject to the initial boundary conditions

$$a_\alpha(-\infty, \boldsymbol{b}) = \delta_{\alpha i}, \quad (9)$$

which assume the atom is initially in the $i = 1s$ state. If the basis states are known, the matrix elements $\langle\psi_\alpha|V|\psi_\beta\rangle$ can be evaluated numerically [28]. We now consider a few kinds of target basis functions.

A. Target description

The description of the target plays an important role in the accuracy and convergence rate of the close-coupling calculations. Since the Coulomb interaction potential between the electron and the proton is spherically symmetric we only consider a solution to the radial Schrödinger equation for a fixed value of the orbital angular momentum l. For negative and positive values of the eigenenergy ε the radial Schrödinger equation has different analytical solutions. For the case when $\varepsilon < 0$, i.e. when the electron stays bound to the proton, the energy of the electron energy has the discrete spectrum with values $\varepsilon_n = -1/(2n^2)$, where n is the principal quantum number. For each discrete value ε_n the radial wave function is given as

$$\varphi_{nl}(r) = \sqrt{\frac{(n-l-1)!}{(n+l)!}}e^{-r/n}\frac{(2r)^{l+1}}{n^{2+l}}L^{2l+1}_{n-l-1}\left(\frac{2r}{n}\right), \quad (10)$$

with $L^{2l+1}_{n-l-1}\left(\frac{2r}{n}\right)$ being the associated Laguerre polynomials. The eigenstate wave functions $\varphi_{nl}(r)$ satisfy the following orthonormality condition:

$$\langle\varphi_{n'l}|\varphi_{nl}\rangle = \int_0^\infty dr\varphi_{n'l}(r)\varphi_{nl}(r) = \delta_{n'n}. \quad (11)$$

When $\varepsilon > 0$, i.e. when the electron is no longer bound to the proton, the radial Schrödinger equation has a continuum of solutions. These continuum functions are written as

$$\varphi_{\kappa l}(r) = \frac{1}{\sqrt{2\pi}}(2\kappa r)^{l+1}\exp\left(\frac{\pi}{2\kappa}\right)\frac{|\Gamma\left(l+1-i/\kappa\right)|}{(2l+1)!} \times e^{-i\kappa r}\,{}_1F_1\left(\frac{i}{\kappa}+l+1, 2l+2, 2irk\right), \quad (12)$$

where $\kappa = \sqrt{2\varepsilon}$ is the momentum of the ejected electron and ${}_1F_1$ is the Kummer confluent hypergeometric function. These functions, known as the Coulomb wave functions, are orthogonal for different values of ε and normalised according to

$$\langle\varphi_{\kappa' l}|\varphi_{\kappa l}\rangle = \int_0^\infty dr\varphi_{\kappa' l}(r)\varphi_{\kappa l}(r) = \delta(\kappa'-\kappa), \quad (13)$$

and satisfy $\langle\varphi_{nl}|\varphi_{kl}\rangle = 0$. In the close-coupling formalism of scattering theory description of the continuum using $\varphi_{\kappa l}(r)$ functions is not possible due to divergent continuum-continuum transition matrix elements. This is because, according to Eq. (13), the true continuum states do not have a finite normalization unlike the bound-state wave functions. For this reason, alternative treatments of the target are used. For comparison, below we briefly describe the Laguerre pseudostates traditionally used in the CCC method, before proceeding to an alternative way of describing the target space using wave packets.

1. *Laguerre pseudostates*

As mentioned above, the target has an infinite number of bound and continuum states. In the scattering equations it is not possible to couple all the channels corresponding to these states. While one can always take a limited number of lowest bound states, the matrix elements corresponding to continuum-continuum transitions diverge as the continuum functions are not square-integrable. Therefore, usually the full set of infinite bound and continuum states of the target is replaced by a suitably-chosen finite set of square-integrable pseudostates. The use of pseudostates eliminates the problem of divergent continuum-continuum V-matrix elements. Also, this allows one to study the convergence of calculated observables in a systematic manner by simply increasing the basis size.

As an example here we will consider a set of pseudostates $\varphi^{\rm L}_{nl}(r)$ generated using the orthogonal square-integrable Laguerre (L) functions. Such a set can be obtained by diagonalising the target Hamiltonian

$$\langle\varphi^{\rm L}_{n'l}|h_{\rm t}|\varphi^{\rm L}_{nl}\rangle = \varepsilon_n\delta_{n'n}, \quad (14)$$

where $h_{\rm t}$ is the radial part of the target Hamiltonian $H_{\rm t}$

$$h_{\rm t} = -\frac{1}{2}\frac{\partial^2}{\partial r^2} - \frac{1}{r}\frac{\partial}{\partial r} + \frac{l(l+1)}{2r^2} - \frac{1}{r}. \quad (15)$$

The pseudostate wave functions are taken as a linear combination

$$\varphi^{\rm L}_{nl}(r) = \sum_{k=1}^{N_l} B^l_{nk}\xi_{kl}(r) \tag{16}$$

of the orthogonal Laguerre functions

$$\xi_{kl}(r) = \left(\frac{\lambda(k-1)!}{(2l+1+k)!}\right)^{1/2}(\lambda r)^{l+1} \times \exp(-\lambda r/2)L^{2l+2}_{k-1}(\lambda r). \tag{17}$$

The fall-off parameter λ is arbitrary and is chosen so that the states with lowest values of n are good approximations for the exact hydrogen eigenfunctions defined by Eq. (10). For convenience in this work we take $\lambda = 2$ for all values of l. In principle, the convergence of the final results is independent of the value of λ. However, inappropriately chosen values of λ can considerably reduce the convergence rate.

Upon diagonalization of the target Hamiltonian $h_{\rm t}$ using pseudostates $\varphi^{\rm L}_{nl}(r)$ one obtaines pseudostate energies ε_{nl}. As in the case with wave functions the energies of the lowest states are essentially equal to the exact values of eigenenergies. In scattering calculations, higher lying negative-energy pseudostates account for the contribution of the infinite number of eigenstates, whereas the contribution of the entire continuum is taken into account by the limited number of positive-energy pseudostates. Note that the full set of the Laguerre pseudostates diagonalising the full target Hamiltonian $H_{\rm t}$ is then written as $\psi^{\rm L}_\alpha(\boldsymbol{r}) = \varphi^{\rm L}_{nl}(r)Y_{lm}(\hat{\boldsymbol{r}})/r$, $\alpha = 1, ..., N$, where Y_{lm} are the spherical harmonics of the unit vector $\hat{\boldsymbol{r}}$. The size of the basis is $N = \sum_{l=0}^{l_{\max}}(2l+1)N_l$, where $l_{\max}$ is the maximum included target orbital angular momentum.

Implementation of this basis yielded excellent results for cross sections of various processes taking place in collisions of light [50–55] and heavy [56–58] projectiles with atomic and molecular targets.

However, in more detailed differential ionization studies of the problem of interest, one needs more dense distribution of states in a particular region of continuum. In such cases the continuum discretization using Laguerre pseudostates becomes inconvenient. Increasing the size of the basis allows one to cover more energies. However, for given fall-off parameter λ, this generates pseudostates of energies too high to be useful. In such a situation reducing the fall-off parameter λ may help reduce the energy of the highest pseudostate. However, this comes at the expense of more pseudostates going to negative energies, thus not helping to increase the density of positive-energy pseudostates. In addition, the energies of continuum pseudostates for different values of l are not aligned. This creates extra difficulties when differential ionization cross sections are calculated. The latter are calculated for each l and need to be interpolated before they are partial-wave summed [59, 60]. To overcome these difficulties, in the next section we will introduce a new way of generating the pseudostates. It allows construction of the basis states with arbitrary energies and distribution.

2. *Wave packets*

To construct normalizable wave packets we first take the continuous spectrum with some maximum value of energy $E_{\max}$ and then divide the whole interval $[0, E_{\max}]$ into $N_{\rm c}$ non-overlapping intervals $[\mathcal{E}_{i-1}, \mathcal{E}_i]_{i=1}^{N_{\rm c}}$ with $\mathcal{E}_0 = 0$ and $\mathcal{E}_{N_{\rm c}} = E_{\max}$. We call the intervals $[\mathcal{E}_{i-1}, \mathcal{E}_i]_{i=1}^{N_{\rm c}}$ the discretization bins. To obtain convergent cross sections, $E_{\max}$ and $N_{\rm c}$ must be sufficiently large. Every such energy bin corresponds to the interval $[\kappa_{i-1}, \kappa_i]$ in momentum space, where $\kappa_i = \sqrt{2\mathcal{E}_i}$. The width of the ith momentum bin is

$$w_i = \kappa_i - \kappa_{i-1}. \tag{18}$$

We define the wave packets corresponding to each of the bins as the normalized integrals of the true continuum functions (Eq. (12)) over the momentum bin region:

$$\varphi^{\rm WP}_{il}(r) = \frac{1}{\sqrt{w_i}}\int_{\kappa_{i-1}}^{\kappa_i} d\kappa\varphi_{\kappa l}(r). \tag{19}$$

It is easy to show that $\varphi^{\rm WP}_{il}(r)$ states are orthonormal:

$$\begin{aligned}\langle\varphi^{\rm WP}_{il}|\varphi^{\rm WP}_{jl}\rangle =& \int_0^\infty dr\varphi^{\rm WP}_{il}(r)\varphi^{\rm WP}_{jl}(r)\\ =&\frac{1}{\sqrt{w_iw_j}}\int_0^\infty dr\int_{\kappa_{i-1}}^{\kappa_i} d\kappa\varphi_{\kappa l}(r)\int_{\kappa_{j-1}}^{\kappa_j} d\kappa'\varphi_{\kappa' l}(r)\\ =&\frac{1}{\sqrt{w_iw_j}}\int_{\kappa_{i-1}}^{\kappa_i} d\kappa\int_{\kappa_{j-1}}^{\kappa_j} d\kappa'\delta(\kappa-\kappa')\\ =&\frac{\delta_{ij}}{\sqrt{w_iw_j}}\int_{\kappa_{i-1}}^{\kappa_i} d\kappa\\ =&\delta_{ij},\end{aligned} \tag{20}$$

where we used Eq. (13). In a similar way it is possible to prove the wave packets also satisfy the following target diagonalization condition

$$\langle\varphi^{\rm WP}_{il}|h_{\rm t}|\varphi^{\rm WP}_{jl}\rangle = \varepsilon_i\delta_{ij}, \tag{21}$$

where ε_i is the middle-energy point of the ith bin, i.e. $\varepsilon_i = (\mathcal{E}_{i-1} + \mathcal{E}_i)/2$. It needs to be emphasized here that the physical meanings of the true Coulomb wavefunction $\varphi_{\kappa l}(r)$ and the normalized discretization-bin wave packet with the same energy $\varphi^{\rm WP}_{il}(r)$ are totally different. The former corresponds to a single state of the continuum, while the latter is constructed from the infinite number of states within a certain region of the continuum. This means the wave packet takes into account the contribution of a certain continuum region, while the true Coulomb wave only a single point which is located in the middle of that region.

Now, by adding $N_{\rm b}$ negative-energy eigenstates we form a WP basis of size N, where the size of the basis is $N = \sum_{l=0}^{l_{\rm max}}(2l+1)(N_{\rm b}-l+N_{\rm c})$. The number of necessary negative-energy eigenstates and WPs representing the target continuum is chosen to give convergent cross sections. The full set of the WP basis states representing the target space is then written as $\psi_\alpha^{\rm WP}(\boldsymbol{r}) = \varphi_{nl}^{\rm WP}(r)Y_{lm}(\hat{\boldsymbol{r}})/r$, $\alpha = 1, ..., N$.

Fig. 1 shows a part of the continuum of atomic hydrogen (shaded area) and corresponding positive-energy wave packets obtained from the energy bins and pseudostates generated by diagonalizing the target Hamiltonian using the Laguerre functions. The displayed WP basis consists of 30 positive-energy states (the same for each l) covering the electron continuum region from 0.05 eV to 400 eV. For ease of comparison on a log scale we have taken the WP bins to grow exponentially in energy, but be the same for each l. Consequently, note that the energy levels of the WP basis are all aligned for different angular momentum symmetries. We also show the positive energy levels of the Laguerre pseudostate basis with 20-l states for each of the l =0 (s), 1 (p) and 2 (d) symmetries. As one can see, for different l the Laguerre energy levels are distributed differently with an uneven distribution of states and fewer states at low energies. This distribution is defined by the size of the basis and the fall-off parameter λ. In contrast, the density of continuum discretization with WP basis is higher everywhere in the covered region below 400 eV. The truncated part of continuum above this energy is negligible since the probability of the electrons being ejected with those energies is extremely low.

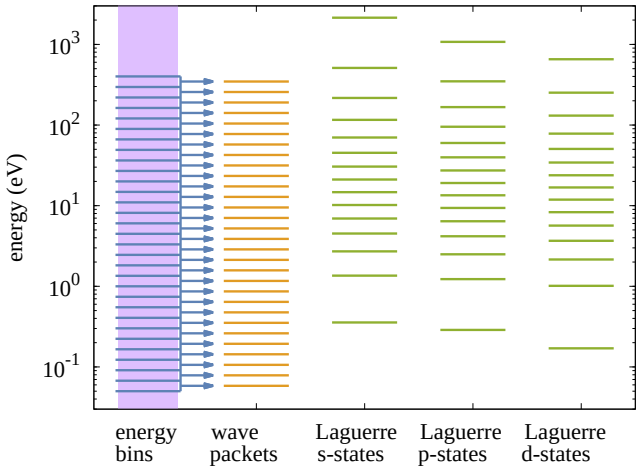

FIG. 1. (color online) The continuum energy levels of atomic hydrogen (shaded area), wave packet bins and resulting energies, as well as Laguerre-based pseudostate energies. The Laguerre pseudostate energies vary with l whereas the wave packet energies do not.

In Fig. 2 we compare the wave packets (normalized to unity) and Laguerre pseudostates, constructed for various values of the ejected electron momentum κ, multiplied by their overlaps with the true Coulomb wave. The corresponding true Coulomb wave functions are also shown. Three values of the ejected electron momentum κ indicated on each of the panels of Fig. 2 correspond to the $n = 10$ states from $l = 0, 1$ and 2 bases of Laguerre functions with the size $20 - l$ and $\lambda = 2$, respectively. The Laguerre pseudostates and the wave packets nearly coincide in some inner domain below $r = 15$ a.u..

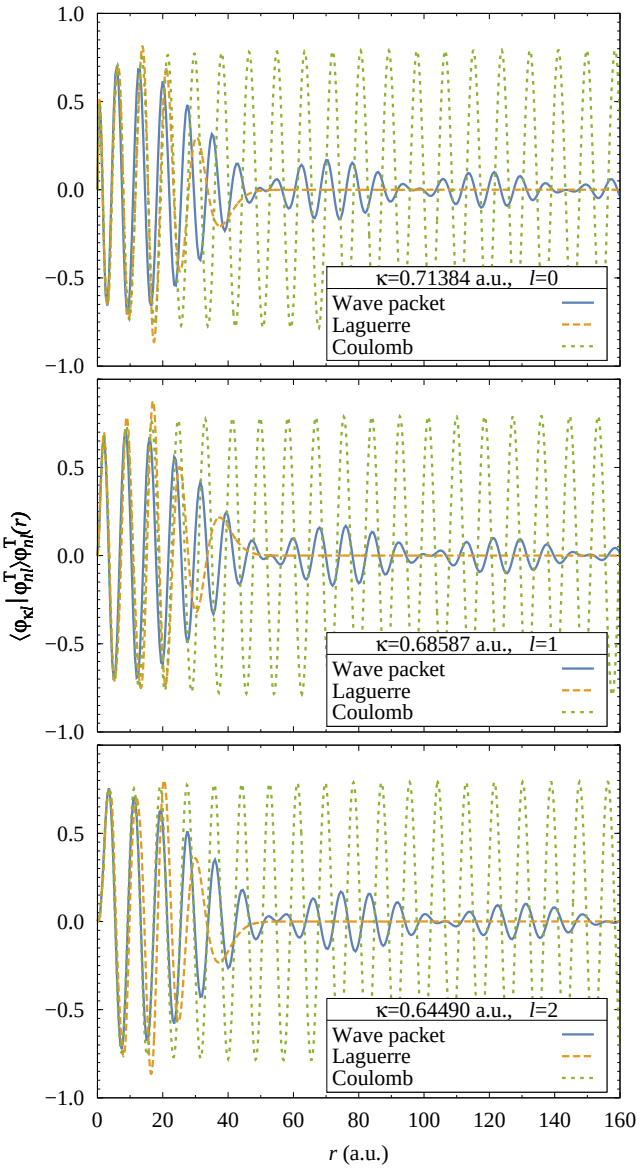

FIG. 2. (color online) The radial dependence of $\langle\varphi_{\kappa l}|\varphi_{nl}^T\rangle\varphi_{nl}^T(r)$ for the wave packets (T=WP) and Laguerre pseudostates (T=L) for various values of the angular momentum l and the ejected electron momentum κ. Also shown are the corresponding true Coulomb wave functions. The wave packets cover the continuum region confined with the bin borders, $\kappa_{\rm min}$ (0.64505 for $l = 0$, 0.61988 for $l = 1$ and 0.58191 for $l = 2$) and $\kappa_{\rm max}$ (0.78263 for $l = 0$, 0.75187 for $l = 1$ and 0.70790 for $l = 2$).

Above $r = 40$ a.u. the Laguerre pseudostates exponentially decay while the wave packets continue their oscillatory behaviour. The agreement between Laguerre pseudostate wave functions and bin wave packets for small values of r is achieved only when the bin boundaries $\kappa_{\rm min} = \kappa - (\kappa - \kappa_{\rm adj})/2$ and $\kappa_{\rm max} = \kappa + (\kappa - \kappa_{\rm adj})/2$, where $\kappa_{\rm adj}$ is the momentum of the lower adjacent Laguerre pseudostate. They are indicated in the figure caption. The Laguerre pseudostate corresponding to κ represents the part of the continuum between $\kappa_{\rm min}$ and $\kappa_{\rm max}$ with an underlying trapezoidal integration rule [61, 62].

B. Cross sections

To be able to calculate various differential cross sections we have to determine the scattering amplitude $T_{fi}(\boldsymbol{q}_f, \boldsymbol{q}_i)$. To this end we use the idea developed in [63]. The amplitude is written in terms of the total scattering wave function Ψ_i^+ as [64]

$$T_{fi}(\boldsymbol{q}_f, \boldsymbol{q}_i) = \langle \Phi_f^- | \overleftarrow{H} - E | \Psi_i^+ \rangle, \tag{22}$$

where Φ_f^- is the asymptotic wave function describing the final state and the arrow over the total three-body Hamiltonian operator H indicates the direction of its action. Eq. (22) is general and applicable for both excitation and breakup of the target. It is also valid for rearrangement channels, however, in the present work we neglect them. If the result of the scattering is excitation of the target then Φ_f^- is given as a product of a plane wave describing the scattered projectile and a bound state wave function of the target in the final state. If the collision leads to ionization of the target then Φ_f^- is a three-body Coulomb asymptotic state described by incoming waves representing the three unbound particles in the final state [65, 66].

The electronic scattering wave function $\Psi_{\rm e}$ [see Eqs. (4) and (7)] is a part of the total scattering wave function Ψ_i^+. As already mentioned our approach is based on the expansion of $\Psi_{\rm e}$ in terms of a set of N square-integrable pseudostates ψ_α. With these we form a projection operator

$$I^N = \sum_{\alpha=1}^{N} |\psi_\alpha^{\rm WP}\rangle\langle\psi_\alpha^{\rm WP}|. \tag{23}$$

Inserting this relation into Eq. (22) we get

$$\begin{aligned} T_{fi}(\boldsymbol{q}_f, \boldsymbol{q}_i) \approx & \langle \Phi_f^- I^N | \overleftarrow{H} - E | I^N \Psi_i^+ \rangle \\ = & \langle \boldsymbol{q}_f \psi_f I^N | V | I^N \Psi_i^+ \rangle \\ = & \langle \psi_f | \psi_f^{\rm WP} \rangle \langle \boldsymbol{q}_f \psi_f^{\rm WP} | V | I^N \Psi_i^+ \rangle \\ \equiv & \langle \psi_f | \psi_f^{\rm WP} \rangle T_{fi}^N(\boldsymbol{q}_f, \boldsymbol{q}_i), \end{aligned} \tag{24}$$

where $\boldsymbol{q}_f$ is the momentum of the scattered projectile and ψ_f is any given state from the full set of the target eigenstates $\{\psi_{nlm}, \psi_{\boldsymbol{\kappa}}^-\}$. Here $\psi_{\boldsymbol{\kappa}}^-$ is the pure incoming Coulomb wave representing the continuum state of the ejected electron with the momentum $\boldsymbol{\kappa}$. In deriving Eq. (24) we took into account that the action of the operator I^N leads to limiting of the target subspace by replacing the full set of the H states (including non-L^2 continuum) with a set of L^2 states. This effectively screens the Coulomb interaction between the projectile and target constituents even in the continuum. We also used the relation that $\langle \psi_f | \psi_\alpha^{\rm WP} \rangle = \delta_{f\alpha} \langle \psi_f | \psi_f^{\rm WP} \rangle$ as by construction we take $\epsilon_f = \epsilon_f^{\rm WP}$ for each target orbital angular momentum l.

We note that when $\psi_f = \psi_{nlm}$ amplitude $T_{fi}^N(\boldsymbol{q}_f, \boldsymbol{q}_i)$ converges to the exact scattering amplitude $T_{fi}(\boldsymbol{q}_f, \boldsymbol{q}_i)$ for excitation of the final nlm state as $N \to \infty$. At the same time when $\psi_f = \psi_{\boldsymbol{\kappa}}^-$ amplitude $T_{fi}^N(\boldsymbol{q}_f, \boldsymbol{q}_i)$ converges to

$$\tilde{T}_{\boldsymbol{\kappa} i}(\boldsymbol{q}_f, \boldsymbol{q}_i) = \langle \boldsymbol{q}_f \psi_{\boldsymbol{\kappa}}^- | V | \Psi_i^+ \rangle, \tag{25}$$

rather than to the exact amplitude of Eq. (22) for breakup. However, it has been demonstrated in [67] that in this case the only difference between the exact amplitude of Eq. (22) and much simpler approximate ionization amplitude of Eq. (25) is a phase factor, i.e. $|T(\boldsymbol{q}_f, \boldsymbol{q}_i)| = |\tilde{T}(\boldsymbol{q}_f, \boldsymbol{q}_i)|$. Therefore, for the purpose of calculating cross sections it is sufficient to know only magnitude of $T_{fi}^N(\boldsymbol{q}_f, \boldsymbol{q}_i)$ for sufficiently large N.

Thus both excitation and ionization amplitudes are obtained upon calculation of transition matrix elements $T_{fi}^N(\boldsymbol{q_f}, \boldsymbol{q_i})$ which are related to the impact-parameter space transition probability amplitudes as follows [68]

$$\begin{aligned} T_{fi}^N(\boldsymbol{q}_f, \boldsymbol{q}_i) = & \frac{1}{2\pi} \int d\boldsymbol{b} e^{i\boldsymbol{p}_\perp \boldsymbol{b}} [a_f(\infty, \boldsymbol{b}) - \delta_{fi}] \\ = & e^{im(\varphi_f + \pi/2)} \int_0^\infty dbb [\tilde{a}_f(\infty, b) - \delta_{fi}] J_m(p_\perp b), \end{aligned} \tag{26}$$

where $\boldsymbol{p} = \boldsymbol{q}_i - \boldsymbol{q}_f$ and $\tilde{a}_f(t, b) = e^{im\phi_{\boldsymbol{b}}} a_f(t, \boldsymbol{b})$.

When $\psi_f = \psi_{nlm}$ we have

$$\langle \psi_{nlm} | \psi_f^{\rm WP} \rangle = 1 \tag{27}$$

by construction. When $\psi_f = \psi_{\boldsymbol{\kappa}}^-$ after partial wave expansion of the 3-dimensional Coulomb wave we easily get

$$\langle \psi_{\boldsymbol{\kappa}}^- | \psi_f^{\rm WP} \rangle = \sqrt{\frac{2}{\pi}} (-i)^l e^{i\sigma_l} b_{nl}(\kappa) Y_{lm}(\hat{\boldsymbol{\kappa}}), \tag{28}$$

where $b_{nl}(\kappa)$ is defined as

$$b_{nl}(\kappa) = \int_0^\infty dr \varphi_{\kappa l}(r) \varphi_{nl}^{\rm WP}(r) = \frac{1}{\sqrt{w_n}}, \tag{29}$$

and σ_l is the Coulomb phase shift. With this it is possible to further simplify Eq. (24) to get

$$T_{\boldsymbol{\kappa} i}(\boldsymbol{q}_f, \boldsymbol{q}_i) = \sum_{l=0}^{l_{\rm max}} \sum_{m=-l}^{l} \frac{(-i)^l e^{i\sigma_l} Y_{lm}(\hat{\boldsymbol{\kappa}}) T_{nlm\,i}^N(\boldsymbol{q}_f, \boldsymbol{q}_i)}{2\pi\kappa\sqrt{w_n}}. \tag{30}$$

Index n in Eqs. (28) - (30) corresponds to the bin with $\kappa = \kappa_n = \sqrt{2\mathcal{E}_n}$.

The most detailed observable, the triply differential cross section (TDCS), can be directly calculated using the ionization amplitude defined in the Eq. (30) as

$$\frac{d^3\sigma(\boldsymbol{\kappa}, \boldsymbol{q}_f, \boldsymbol{q}_i)}{dE d\Omega_e d\Omega_f} = \mu^2 \frac{q_f \kappa}{q_i} |T_{\boldsymbol{\kappa} i}(\boldsymbol{q}_f, \boldsymbol{q}_i)|^2, \tag{31}$$

where μ is the reduced mass of the projectile-target system. This cross section is for the electron being ejected into the solid angle $d\Omega_e$ with the energy in the range E to $E + dE$, where $E = \kappa^2/2$, when the projectile is incident along the quantization axis z ($\boldsymbol{q}_i \parallel z$) and further scattered into the solid angle $d\Omega_f$.

Two types of doubly-differential cross sections (DDCS) are usually used. The first one can be obtained by integrating the TDCS over the spherical coordinates of the scattered projectile:

$$\begin{aligned}\frac{d^2\sigma(\boldsymbol{\kappa}, q_f, q_i)}{dE d\Omega_e} =& \int \frac{d^3\sigma(\boldsymbol{\kappa}, \boldsymbol{q}_f, q_i)}{dE d\Omega_e d\Omega_f} d\Omega_f \\ =& \frac{\mu^2}{2\pi q_i^2 \kappa w_n} \sum_{l=0}^{l_{\max}} \sum_{l'=0}^{l} \sum_{m=-l'}^{l'} \frac{2}{1+\delta_{l'l}} \\ & \times Y_{lm}(\hat{\boldsymbol{\kappa}}) Y^*_{l'm}(\hat{\boldsymbol{\kappa}}) \mathrm{Re}\Bigg[(-i)^{l-l'} e^{i(\sigma_l - \sigma_{l'})} \\ & \times \int_0^\infty dbb \tilde{a}_{nlm}(\infty, b) \tilde{a}^*_{nl'm}(\infty, b)\Bigg],\end{aligned} \tag{32}$$

where we assumed

$$\int d\Omega_f = \frac{1}{q_f q_i} \int_0^{2\pi} d\varphi_f \int_0^\infty dp_\perp p_\perp$$

and used the identity

$$\int_0^\infty dp_\perp p_\perp J_m(p_\perp b) J_m(p_\perp b') = \frac{\delta(b-b')}{b}.$$

The DDCS defined this way shows the angular and energy distributions of the ejected electrons. Another DDCS can be formed by integrating the TDCS over the spherical coordinates of the ejected electron (this can be done analytically) and is written as

$$\begin{aligned}\frac{d^2\sigma(\kappa, \boldsymbol{q}_f, q_i)}{dE d\Omega_f} =& \int \frac{d^3\sigma(\boldsymbol{\kappa}, \boldsymbol{q}_f, q_i)}{dE d\Omega_e d\Omega_p} d\Omega_e \\ =& \frac{\mu^2 q_f}{4\pi^2 q_i \kappa w_n} \sum_{l=0}^{l_{\max}} \sum_{m=-l}^{l} |T_{\boldsymbol{\kappa} i}(\boldsymbol{q}_f, \boldsymbol{q}_i)|^2.\end{aligned} \tag{33}$$

This cross section is differential in the angular variables of the scattered projectile and the energy of the ejected electron.

The singly differential cross section (SDCS) in the energy of the ejected electron can be calculated by integrating Eq. (33) over Ω_f. Integration of Eq. (33) over Ω_f gives us

$$\frac{d\sigma(\kappa, q_f, q_i)}{dE} = \frac{1}{\kappa w_n} \sum_{l=0}^{l_{\max}} \sum_{m=-l}^{l} \sigma_{nlm}, \tag{34}$$

where σ_{nlm} is the cross section for excitation of the pseudostate in channels $f = \{nlm\}$. The latter is calculated as

$$\sigma_{nlm} = 2\pi \int_0^{b_{\max}} dbb P_{nlm}(b), \tag{35}$$

where $b_{\max}$ is the upper limit for the impact parameter. It will be specified in the next section. The transition probability is calculated as

$$P_{nlm}(b) = |a_{nlm}(+\infty, \boldsymbol{b}) - \delta_{nlm,1s}|^2. \tag{36}$$

Alternatively, the SDCS in the momentum of the ejected electron can be defined as

$$\frac{d\sigma(\kappa, q_f, q_i)}{d\kappa} = \frac{1}{w_n} \sum_{l=0}^{l_{\max}} \sum_{m=-l}^{l} \sigma_{nlm}. \tag{37}$$

The SDCS in the electron ejection angle, $d\sigma/d\Omega_e$, can be obtained from integration of $d\sigma/dE/d\Omega_e$ over dE, i.e.

$$\begin{aligned}\frac{d\sigma}{d\Omega_e} =& \frac{\mu^2}{2\pi q_i^2} \sum_{n=N_\mathrm{b}+1}^{N_\mathrm{b}+N_\mathrm{c}} \sum_{l=0}^{l_{\max}} \sum_{l'=0}^{l} \sum_{m=-l'}^{l'} \frac{2}{1+\delta_{l'l}} \\ & \times Y_{lm}(\hat{\boldsymbol{\kappa}}) Y^*_{l'm}(\hat{\boldsymbol{\kappa}}) \mathrm{Re}\Bigg[(-i)^{l-l'} e^{i(\sigma_l - \sigma_{l'})} \\ & \times \int_0^\infty dbb \tilde{a}_{nlm}(\infty, b) \tilde{a}^*_{nl'm}(\infty, b)\Bigg].\end{aligned} \tag{38}$$

Finally, the total integrated ionization cross section is written as

$$\sigma_{\mathrm{ion}} = \sum_{n=N_\mathrm{b}+1}^{N_\mathrm{b}+N_\mathrm{c}} w_n \frac{d\sigma(\kappa, q_f, q_i)}{d\kappa} = \sum_{n=N_\mathrm{b}+1}^{N_\mathrm{b}+N_\mathrm{c}} \sum_{l=0}^{l_{\max}} \sum_{m=-l}^{l} \sigma_{nlm}. \tag{39}$$

III. DETAILS OF CALCULATIONS

In the previous section we derived expressions to calculate various differential cross sections. Before proceeding further we give some details of our calculations. To ensure the convergence of calculations several parameters associated with the target and the projectile need to be investigated. Parameters defining the target structure are the maximum allowed orbital quantum number $l_{\max}$, the number of bound (negative-energy) eigenstates $N_\mathrm{b} - l$, the maximum energy $E_{\max}$ of the electron continuum covered by wave-packet bins, and the number of bins within this interval N_c. Convergence of the final results is studied by systematically increasing each of these

parameters while fixing the others at sufficiently large values. This procedure is continued until the parameter-dependent variation of the results is reduced to a level less than one percent. At intermediate and high energies this is achieved with $l_{\max} = 10$, $N_{\rm b} = 10 - l$, $E_{\max} = 400$ eV and $N_{\rm c} = 30$. It is this basis depicted in Figure 1. However, at lower projectile energies we had to increase the number of wave packets and reduce $E_{\max}$. To be specific, at 2 keV we had $N_{\rm c} = 90$ and $E_{\max} = 40$ eV. With these parameters the total number of target states N in the present calculations was from 4015 at high energies to 11275 at low energies. The total number of basis states also defines the size of the set of the coupled differential equations (8). To ensure that the employed basis was sufficiently large we were also guided by the analytical first Born (FBA) results obtained in the full wave treatment [69]. Before performing full calculations we obtained excellent agreement with the first Born results when coupling between discretised channels was switched off.

The number of quadrature points for integration within each bin was taken to provide an adequate accuracy and chosen depending on the width of the bin. Typically, at least 40 points were used for the smallest bins and increased for larger bins as required.

It is noteworthy to comment on the structure treatment implemented in our previous QM-CCC calculations [28, 48]. The QM-CCC calculations utilised the orthogonal Laguerre basis (16) with parameters $N_l = 20-l$, $l_{\max} = 5$ and $\lambda = 2$. The state energies of this target basis are displayed in Fig. 1 for orbital angular-momentum quantum numbers $l = 0$, 1 and 2. While both the present bin-based WP-CCC and the previous Laguerre-based QM-CCC approaches allow one to study the convergence of the results by increasing the number of the target states, the present formulation has the advantage of being able to explicitly choose a specific positive energy, and for this to be the same for each l. This is helpful in differential ionization studies where the outgoing electron energy is specified. Furthermore, the bin-based formulation has considerably greater flexibility in the way the energies can be distributed.

The convergence of calculations with varying parameters associated with the projectile has been carefully studied. The set of coupled differential equations (8) was solved by varying the z-component ($z \equiv vt$) of the projectile position from -200 to $+200$ a.u. at all energies. The upper limit for the impact parameter $b_{\max}$ is proportionally increased from 10 a.u. at 1 keV and to 40 a.u. at 1 MeV [70]. The radial grid required for calculations of the matrix elements was 500 a.u. at the highest energy and 2000 a.u. at the lowest energy.

Finally, during the calculations we always make sure that we obtain exactly the same total ionization cross section both by summing over the partial cross sections for excitation of the positive-energy states (equation (39)) and by integrating the fully differential cross section $d^3\sigma/dE/d\Omega_e/d\Omega_p$ (equation (31)) over all variables.

IV. RESULTS AND DISCUSSION

In this section we present our numerical results for triply, doubly, and singly differential ionization cross sections, as well as the total ionization cross section. Collision geometries and projectile energies are chosen in such a way that allows the most comprehensive comparison with our quantum-mechanical CCC results published in Refs. [28, 48] and other semiclassical theories [6, 29, 30, 44]. In addition we present results for differential cross sections and kinematic regimes which have not been previously considered.

A. Triply differential cross sections

In Figure 3 we show our results for the triply differential cross section in the collision plane. The present WP-CCC results are compared with our previous QM-CCC results, the Born approximation, the continuum-distorted-wave eikonal-initial-state (CDW-EIS) calculations of Voitkiv and Ullrich [6] and coupled-pseudostate (CP) calculations of McGovern *et al.* [30]. Here we fix the direction of scattered antiprotons and show the value of the momentum transfer $\boldsymbol{p}$, while the electron ejection angle $\theta_{\rm e}$ runs from -180° to 180° relative to the direction of the incident antiproton. Since the coplanar geometry is considered the azimuthal coordinates of the ejected electron $\phi_{\rm e}$ and the antiproton ϕ_f are set to 0. The arrow indicates the direction of momentum transfer. We note that the results of other approaches are transformed to the collision geometry and coordinate frame that we have currently adopted. The ejected electron energy is fixed at 5 eV. The flexibility of the presently developed WP basis in distributing positive energy states arbitrarily allowed us to have a state with the energy exactly equal to 5 eV for all l. This was not possible in the QM-CCC calculations where we had to calculate the TDCS at 5 eV by interpolating the TDCS at other available energies.

As one can see from the figure, for every indicated antiproton energy and momentum transfer our current WP-CCC and previous QM-CCC results are generally in good agreement. As discussed earlier, slight disagreement at $E_{\rm p} = 30$ keV and 214.84 keV (corresponds to projectile speed of 3 a.u.) is due to insufficient density of positive-energy pseudostates around 5 eV in the Laguerre basis (see Fig. 1) utilised in our previous QM-CCC calculations. At 500 keV both WP-CCC and QM-CCC are in good agreement with the coupled-pseudostate calculations of McGovern *et al.* [30], and the CDW-EIS calculations of Voitkiv and Ullrich [6]. Here even the Born approximation is reasonably accurate. At every projectile energy all presented theories predict the binary and recoil peaks at the same electron ejection angle which qualitatively describes the phenomenon of suppressed electron ejection in the direction of the scattered antiprotons (essentially zero degrees). Due to the repulsive Coulomb force between the antiproton and electron the binary

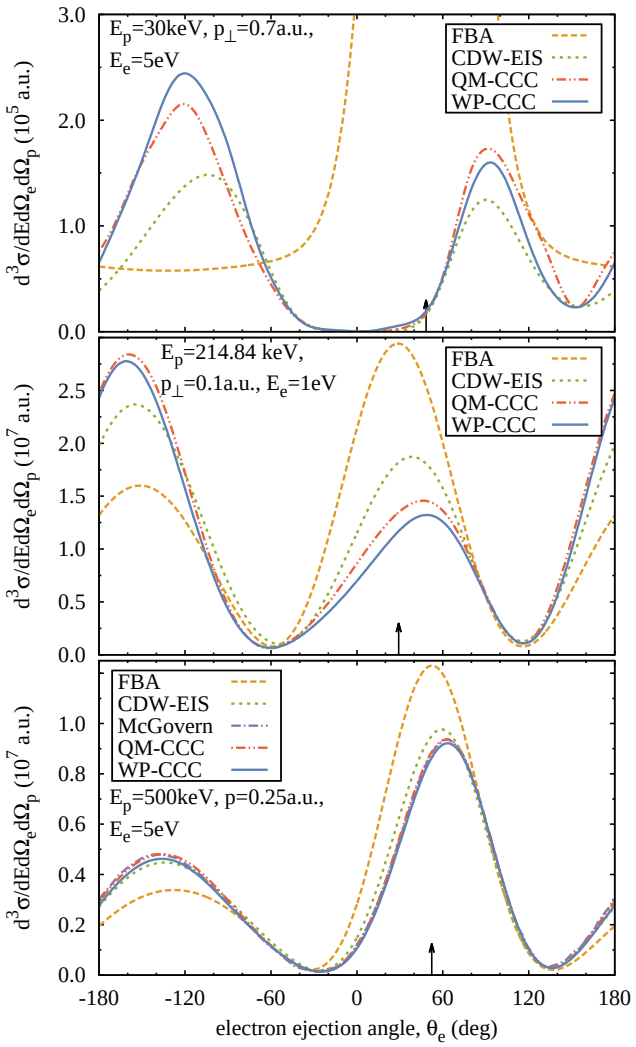

FIG. 3. (color online) Triply differential cross sections for antiproton-impact ionization of the ground state of atomic hydrogen at various scattering angles and energies of the ejected electron for specified projectile energies E_p. Results of the QM-CCC, CDW-EIS and semiclassical CP approaches are due to [48], [6] and [30], respectively. The arrows indicate the direction of the momentum transfer.

peak is shifted to the right from the momentum transfer direction. Note that the Born approximation is always symmetric around the momentum transfer direction.

It is interesting to observe how drastically the TDCS at a particular scattering angle changes as a function of the incident energy. An example is given in Figure 4 for the TDCS at 0° scattering angle of the projectile at low and high incident energies. As one can see, at high projectile energies the electron ejection peaks in both forward and backward directions. However, as the incident energy falls the forward ejection is completely suppressed. Again, this is due to the repulsive Coulomb interaction

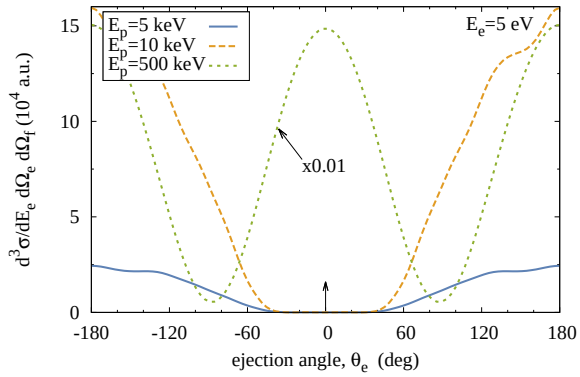

FIG. 4. (color online) Triply differential cross sections for antiproton-impact ionization of the ground state of atomic hydrogen at specified projectile energies E_p. The ejected electron energy is 5 eV, and the antiproton is scattered to 0°.

between ejected electron and antiproton.

Fig. 5 presents the TDCS at various scattering angles of the projectile and ejected-electron energies for 75 keV antiproton impact. Though the variation of the projectile angle is rather small, in steps of 0.1 mrad, the effect on the TDCS is rather large at all considered electron ejection energies, which were chosen to correspond to energy losses of 30 eV, 40 eV, 50 eV, and 53 eV according to the experimental setup for proton scattering DDCS Laforge *et al.* [71].

B. Doubly differential cross sections

The DDCS in energy of the ejected electron and scattered angle of the projectile, $\mathrm{d}^2\sigma/\mathrm{d}E/\mathrm{d}\Omega_f$, are shown in Fig. 6 at the same electron energies as for Fig. 5. The corresponding proton-impact DDCS of [71] are rather different from the antiproton-impact ones shown, and are not presented. At the intermediate energy of 75 keV the proton-impact electron capture cross section is very large, and so it is not surprising that the DDCS would be very different for antiproton impact. We look forward to calculating proton-impact TDCS and DDCS utilising the two-centre bin-based CCC formalism for heavy projectiles.

The DDCS in energy and angle of the ejected electron, $\mathrm{d}^2\sigma/\mathrm{d}E/\mathrm{d}\Omega_\mathrm{e}$, are presented in Figure 7 for the ejected electron energy of $E_\mathrm{e} = 5$ eV and various energies of the incident antiproton as a function of the electron ejection angle θ_e. The QM-CCC results and the results of the coupled-pseudostate approach of McGovern *et al.* [30] are also presented for comparison. Since this cross section is formed as a result of integration of the TDCS over the scattering angle of the projectile, the DDCS results displayed in Fig. 7 retain some features of the corresponding TDCS shown in Fig. 3. As expected, the electron emission is negligible at small ejection angles. The pro-

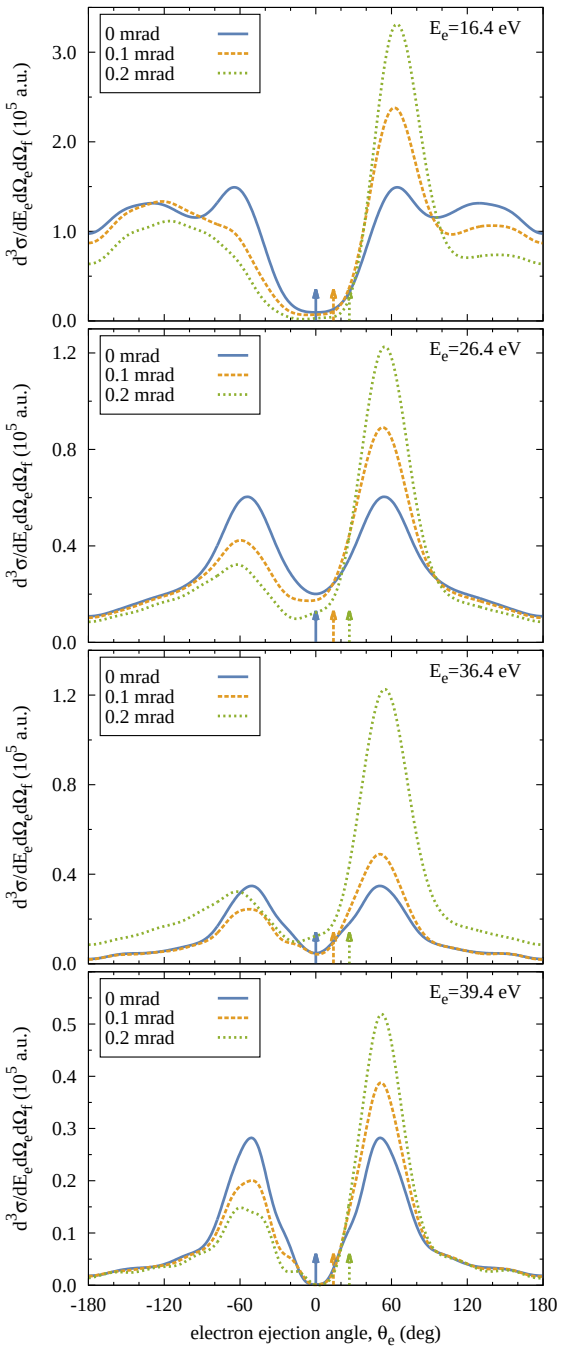

FIG. 5. (color online) 75 keV antiproton-impact ionization of the ground state of hydrogen TDCS at the specified scattering angles of the projectile and ejected-electron energies E_e. The arrows indicate the momentum transfer direction.

nounced peaks at around 80° and the shallow peaks at 180° are the integral results of the binary and recoil peaks of the TDCS, respectively. Small difference between the WP-CCC and QM-CCC results can again be attributed to the lack of Laguerre pseudostates with energies close to 5 eV in the QM-CCC calculations.

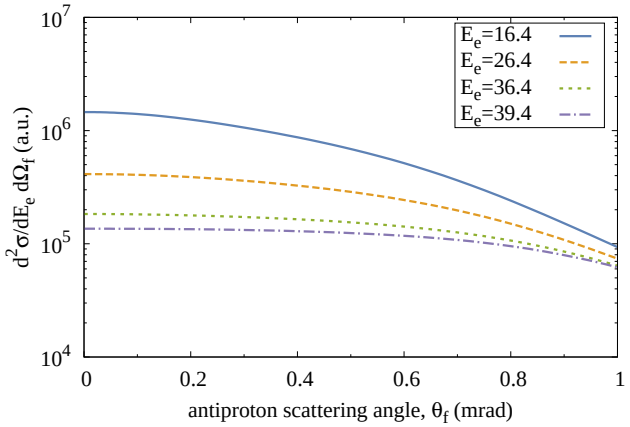

FIG. 6. (color online) The $d^2\sigma/dE/d\Omega_f$ at specified ejected-electron energies for 75 keV antiproton impact.

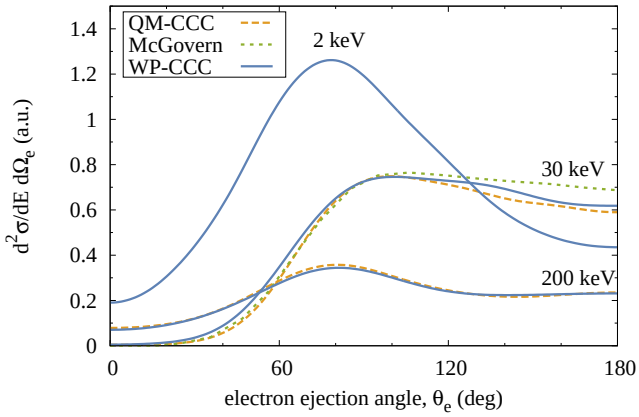

FIG. 7. (color online) The $d^2\sigma/dE/d\Omega_e$ for antiproton-impact ionization of hydrogen at 30, 200 and 500 keV for an ejected electron of 5 eV. Results of the QM-CCC approach and the coupled pseudostates approach of McGovern *et al.* [30] are also presented for comparison.

C. Singly differential cross sections

In Fig. 8 we show our results for the SDCS in the ejection angle of the electron, $d\sigma/d\Omega_e$, in comparison with our other available calculations. Except for the lowest energy considered, the cross section is lowest in the forward direction has maximum around 60° and a minimum around 120°. The relatively large cross section in the backward direction at all considered energies indicates the propensity for the electron to be ejected in the opposite direction to the antiproton. The agreement between the present WP-CCC results and the semiclassical approaches of Igarashi *et al.* [29] and McGovern *et al.* [44] is somewhat variable, but improves with increasing energy.

The SDCS in the energy of the ejected electron is pre-

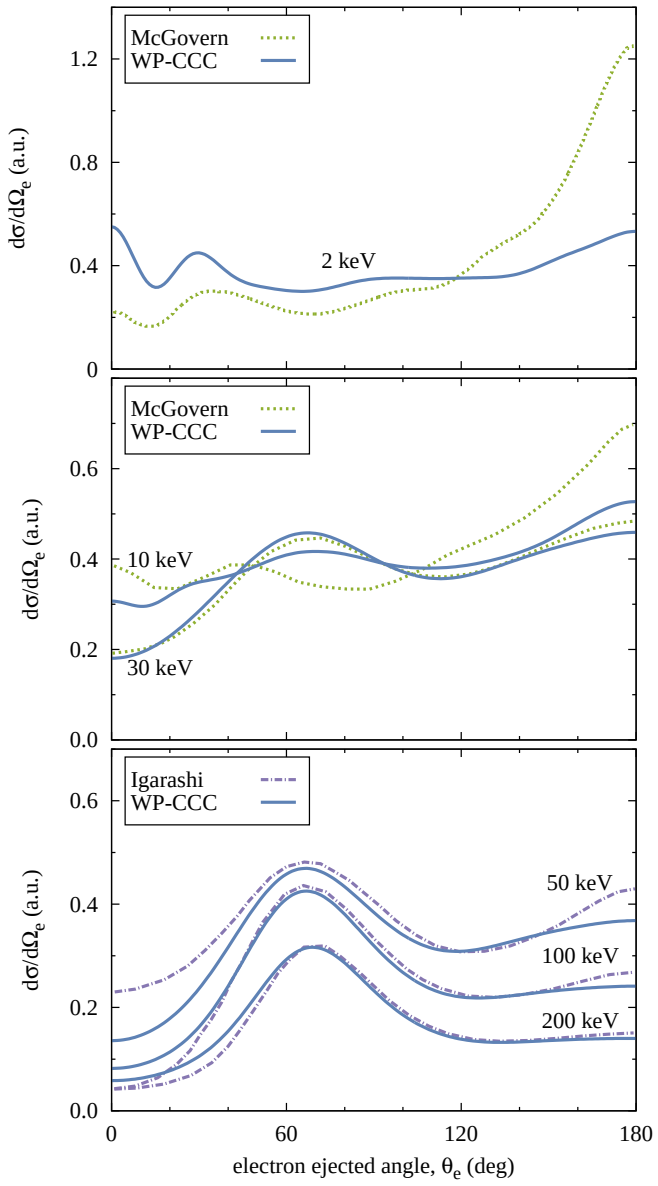

FIG. 8. (color online) The singly differential cross section in the electron ejection angle at incident energies of antiproton 2–200 keV. Results of semiclassical CC approaches are due to Igarashi *et al.* [29] and McGovern *et al.* [44].

sented in Fig. 9. Previously, the QM-CCC results [48] and the coupled-pseudostate calculations [30] predicted cross sections to monotonically decrease with the increasing electron ejected energy at all considered projectile energies. However, the present WP-CCC results exhibit a qualitatively different behavior at low electron ejection energies, with the SDCS rising rapidly towards a maximum. This is most prevalent at the lowest impact energies presented. We checked this result in a model problem which retained only s-states of hydrogen, using both the WP-CCC and QM-CCC approaches, and such behavior was also evident there. Absence of the low energy peaks in our previous QM-CCC results is attributed to the fact that in these calculations the discretization of the low-energy part of the continuum was insufficient to reveal the fine details. This is seen in Fig. 1 where below 2 eV the Laguerre basis has just two states. We suppose the same conclusion is applicable to the coupled-pseudostate results of McGovern *et al.* [30] as well. As mentioned in Section III, at low incident energies we used 90 bins for ejected electron energy range from 0 to 40 eV. The resulting wave-packet basis had 19 states below 2 eV. The present Born calculations are given just as a check that the WP basis is behaving as expected if coupling is turned off.

D. Total ionization cross section

Finally, in Fig. 10 we show our results for the total ionization cross section in comparison with the experimental data of Knudsen *et al.* [72], the quantum-mechanical CCC results and other semiclassical calculations [29, 30, 33] for the incident energies ranging from 1 keV to 1 MeV. The calculated WP-CCC cross sections are in excellent agreement both with the experiment and the QM-CCC results. There is insignificant variation between the WP-CCC and QM-CCC results at the energy range from 2 keV to 10 keV which is a couple of percents at most. As discussed earlier, this is due to the deficiency of the basis used in the QM-CCC calculations since the continuum discretization using Laguerre pseudostates is significantly sparser than the discretisation density resulting from the present wave packets. Overall, the present results for TICS are in good agreement with other semiclassical close-coupling calculations [29, 30, 33].

V. CONCLUSIONS AND FUTURE OUTLOOK

A new continuum-discretization approach to ion-atom collisions based on stationary wave packets has been developed. The normalized wave packets constructed from the radial Coulomb wave functions have been used to discretize the continuous spectrum of the target. The generated orthonormal wave-packet basis is used in the target-based one-center expansion of the total scattering wave function. This converts the semiclassical three-body Schrödinger equation into a set of coupled-channel differential equations. One of the favorable features of the developed method is the ability of generating target states with arbitrary energies and distribution. This, in addition to improving the accuracy of the calculations, also has a particular advantage in calculating differential ionization cross sections where the energies of the pseudostates with different orbital quantum number are aligned naturally. The density of the continuum discretisation can be as high as necessary.

The utility of the new method is demonstrated on the

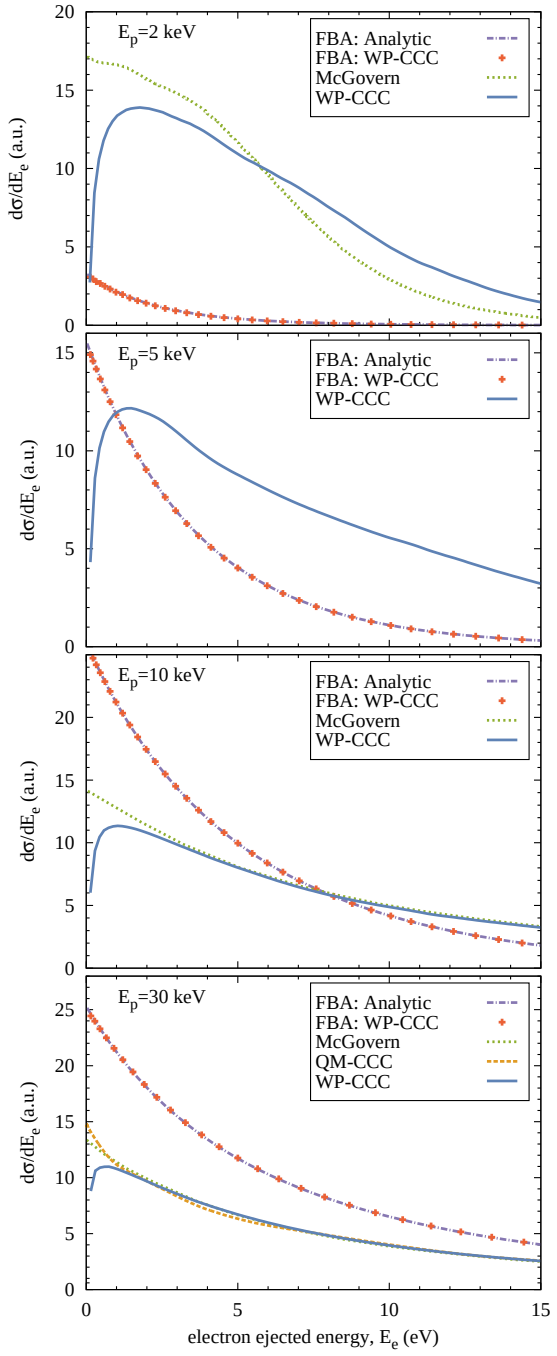

FIG. 9. (color online) The singly differential cross section in the ejection energy of the electron at various projectile energies. Results of the QM-CCC approach and the semiclassical coupled pseudostates approach are due to Abdurakhmanov *et al.* [48] and McGovern *et al.* [30], respectively.

example of antiproton collisions with atomic hydrogen. The integrated, fully differential, as well as various doubly and singly differential cross sections for antiproton-impact ionization of hydrogen have been calculated and a comprehensive set of highly-accurate benchmark results have been presented. Data for other channels not considered here, and arbitrary kinematic regimes can be provided upon request.

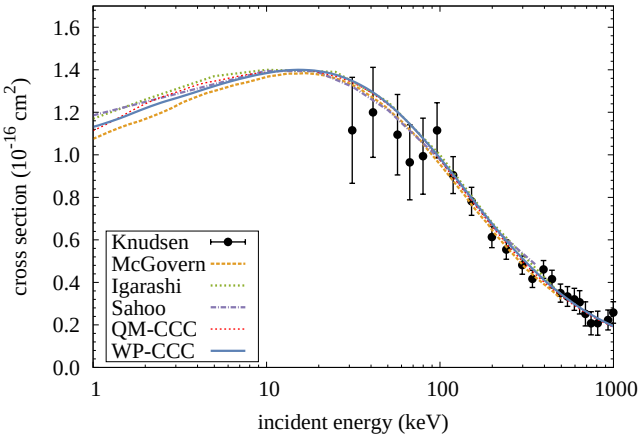

FIG. 10. (color online) Total ionization cross section for antiproton-hydrogen scattering. Present calculations (WP-CCC) are compared with experimental data by Knudsen *et al.* [72], quantum mechanical convergent-close-coupling (QM-CCC) results [28], and various semiclassical calculations of McGovern *et al.* [30], Igarashi *et al.* [29] and Sahoo *et al.* [33].

Extension of the developed wave-packet continuum-discretisation approach to the two-center rearrangement problems including electron capture will be reported in the second part of the work. The ability of the approach of generating target states with arbitrary energies and distribution allows one to investigate the issues associated with the nonorthogonality of the two-center expansion basis and double-counting of the continuum.

The developed wave-packet convergent close-coupling method is not limited to hydrogen-like targets. It can be extended to more complicated atomic and molecular targets.

ACKNOWLEDGMENTS

The work was supported by the Australian Research Council. We are grateful for access to the Australian National Computing Infrastructure Facility and the Pawsey Supercomputing Centre in Western Australia. A.S.K. acknowledges a partial support from the U.S. National Science Foundation under Award No. PHY-1415656.

[1] D. Belkić, Journal of Mathematical Chemistry **47**, 1366 (2010).

[2] A. Igarashi and C. D. Lin, Phys. Rev. Lett. **83**, 4041

(1999).
[3] S. Zou, L. Pichl, M. Kimura, and T. Kato, Phys. Rev. A **66**, 042707 (2002).
[4] P. D. Fainstein, V. H. Ponce, and R. D. Rivarola, J. Phys. B **24**, 3091 (1991).
[5] F. D. Colavecchia, G. Gasaneo, and C. R. Garibotti, Journal of Physics B: Atomic, Molecular and Optical Physics **33**, L467 (2000).
[6] A. B. Voitkiv and J. Ullrich, Phys. Rev. A **67**, 062703 (2003).
[7] D. Belkic, *Quantum Theory of High-Energy Ion-Atom Collisions* (CRC Press, 2008).
[8] H. A. Slim and A. M. Ermolaev, Journal of Physics B: Atomic, Molecular and Optical Physics **27**, L203 (1994).
[9] J. Kuang and C. D. Lin, J. Phys. B **29**, 5443 (1996).
[10] N. Toshima, Phys. Rev. A **59**, 1981 (1999).
[11] M. Keim, A. Werner, D. Hasselkamp, K.-H. Schartner, H. J. Luedde, A. Achenbach, and T. Kirchner, Journal of Physics B: Atomic, Molecular and Optical Physics **38**, 4045 (2005).
[12] T. G. Winter, Phys. Rev. A **80**, 032701 (2009).
[13] H. R. J. Walters and C. T. Whelan, Phys. Rev. A **92**, 062712 (2015).
[14] D. R. Schultz, M. R. Strayer, and J. C. Wells, Phys. Rev. Lett. **82**, 3976 (1999).
[15] A. Kołakowska, M. S. Pindzola, and D. R. Schultz, Phys. Rev. A **59**, 3588 (1999).
[16] M. Chassid and M. Horbatsch, Phys. Rev. A **66**, 012714 (2002).
[17] G. V. Avakov, A. R. Ashurov, L. D. Blokhinstev, A. M. Mukhamedzhanov, and M. V. Poletayeva, J. Phys. B **23**, 2309S (1990).
[18] G. V. Avakov, A. R. Ashurov, L. D. Blokhintsev, A. S. Kadyrov, A. M. Mukhamedzhanov, and M. V. Poletayeva, J. Phys. B **23**, 4151 (1990).
[19] G. V. Avakov, L. D. Blokhintsev, A. S. Kadyrov, and A. M. Mukhamedzhanov, J. Phys. B **25**, 213 (1992).
[20] E. O. Alt, G. V. Avakov, L. D. Blokhintsev, A. S. Kadyrov, and A. M. Mukhamedzhanov, J. Phys. B **27**, 4653 (1994).
[21] E. O. Alt, A. S. Kadyrov, and A. M. Mukhamedzhanov, Phys. Rev. A **60**, 314 (1999).
[22] I. B. Abdurakhmanov, A. S. Kadyrov, D. V. Fursa, S. K. Avazbaev, J. J. Bailey, and I. Bray, Phys. Rev. A **91**, 022712 (2015).
[23] S. K. Avazbaev, A. S. Kadyrov, I. B. Abdurakhmanov, D. V. Fursa, and I. Bray, Phys. Rev. A **93**, 022710 (2016).
[24] I. B. Abdurakhmanov, A. S. Kadyrov, and I. Bray, J. Phys. B **49**, 03LT01 (2016).
[25] I. B. Abdurakhmanov, A. S. Kadyrov, S. K. Avazbaev, and I. Bray, J. Phys. B **49**, 115203 (2016).
[26] K. A. Hall, J. F. Reading, and A. L. Ford, J. Phys. B **29**, 6123 (1996).
[27] B. Pons, Phys. Rev. Lett. **84**, 4569 (2000).
[28] I. B. Abdurakhmanov, A. S. Kadyrov, I. Bray, and A. T. Stelbovics, J. Phys. B **44**, 075204 (2011).
[29] A. Igarashi, S. Nakazaki, and A. Ohsaki, Phys. Rev. A **61**, 062712 (2000).
[30] M. McGovern, D. Assafrão, J. R. Mohallem, C. T. Whelan, and H. R. J. Walters, Phys. Rev. A **79**, 042707 (2009).
[31] N. Toshima, Phys. Rev. A **64**, 024701 (2001).
[32] J. Azuma, N. Toshima, K. Hino, and A. Igarashi, Phys. Rev. A **64**, 062704 (2001).
[33] S. Sahoo, S. C. Mukherjee, and H. R. J. Walters, J. Phys. B **37**, 3227 (2004).
[34] H. Weyl, Mathematische Annalen **68**, 220 (1910).
[35] E. Wigner and J. Griffin, *Group Theory and Its Application to the Quantum Mechanics of Atomic Spectra*, Pure and applied Physics (Academic Press, 1959).
[36] H. Bethe, *Quantenmechanik der Ein- und Zwei-Electronenprobleme*, Handbuch der Physik, Zweite Auflage, XXIV (Erster Teil, 1933).
[37] N. Austern, Y. Iseri, M. Kamimura, M. Kawai, G. Rawitscher, and M. Yahiro, Phys. Rep. **154**, 125 (1987).
[38] V. I. Kukulin and O. A. Rubtsova, Theor. Math. Phys. **130**, 54 (2002).
[39] O. Rubtsova, V. Kukulin, and V. Pomerantsev, Annals of Physics **360**, 613 (2015).
[40] G. Schiwietz, Phys. Rev. A **42**, 296 (1990).
[41] I. B. Abdurakhmanov, A. S. Kadyrov, D. V. Fursa, and I. Bray, Phys. Rev. Lett. **111**, 173201 (2013).
[42] I. B. Abdurakhmanov, A. S. Kadyrov, D. V. Fursa, S. K. Avazbaev, and I. Bray, Phys. Rev. A **89**, 042706 (2014).
[43] M. H. Martir, A. L. Ford, J. F. Reading, and R. L. Becker, J. Phys. B **15**, 1729 (1982).
[44] M. McGovern, D. Assafrão, J. R. Mohallem, C. T. Whelan, and H. R. J. Walters, Phys. Rev. A **81**, 032708 (2010).
[45] D. R. Schultz, P. S. Krstic, C. O. Reinhold, and J. C. Wells, Phys. Rev. Lett. **76**, 2882 (1996).
[46] J. C. Wells, D. R. Schultz, P. Gavras, and M. S. Pindzola, Phys. Rev. A **54**, 593 (1996).
[47] X.-M. Tong, T. Watanabe, D. Kato, and S. Ohtani, Phys. Rev. A **64**, 022711 (2001).
[48] I. B. Abdurakhmanov, A. S. Kadyrov, I. Bray, and A. T. Stelbovics, J. Phys. B **44**, 165203 (2011).
[49] B. H. Bransden and M. R. C. McDowell, *Charge Exchange and the Theory of Ion-Atom Collisions* (Clarendon, Oxford, 1992).
[50] A. S. Kadyrov and I. Bray, Phys. Rev. A **66**, 012710 (2002).
[51] A. S. Kadyrov, C. M. Rawlins, A. T. Stelbovics, I. Bray, and M. Charlton, Phys. Rev. Lett. **114**, 183201 (2015).
[52] C. M. Rawlins, A. S. Kadyrov, A. T. Stelbovics, I. Bray, and M. Charlton, Phys. Rev. A **93**, 012709 (2016).
[53] A. W. Bray, I. B. Abdurakhmanov, A. S. Kadyrov, D. V. Fursa, and I. Bray, Comp. Phys. Comm. **196**, 276 (2015).
[54] A. W. Bray, I. B. Abdurakhmanov, A. S. Kadyrov, D. V. Fursa, and I. Bray, Comp. Phys. Comm. **203**, 147 (2016).
[55] M. C. Zammit, J. S. Savage, D. V. Fursa, and I. Bray, Phys. Rev. Lett. **116**, 233201 (2016).
[56] I. B. Abdurakhmanov, A. S. Kadyrov, D. V. Fursa, I. Bray, and A. T. Stelbovics, Phys. Rev. A **84**, 062708 (2011).
[57] J. J. Bailey, A. S. Kadyrov, I. B. Abdurakhmanov, D. V. Fursa, and I. Bray, Phys. Rev. A **92**, 022707 (2015).
[58] J. J. Bailey, A. S. Kadyrov, I. B. Abdurakhmanov, D. V. Fursa, and I. Bray, Phys. Rev. A **92**, 052711 (2015).
[59] I. Bray and D. V. Fursa, Phys. Rev. A **54**, 2991 (1996).
[60] I. Bray, D. V. Fursa, A. S. Kadyrov, A. T. Stelbovics, A. S. Kheifets, and A. M. Mukhamedzhanov, Phys. Rep. **520**, 135 (2012).
[61] B. H. Bransden and A. T. Stelbovics, J. Phys. B **17**, 1877 (1984).

[62] D. A. Konovalov, I. Bray, and I. E. McCarthy, J. Phys. B **27**, L413 (1994).
[63] A. S. Kadyrov, J. J. Bailey, I. Bray, and A. T. Stelbovics, Phys. Rev. A **89**, 012706 (2014).
[64] A. S. Kadyrov, I. Bray, A. M. Mukhamedzhanov, and A. T. Stelbovics, Phys. Rev. Lett. **101**, 230405 (2008).
[65] E. O. Alt and A. M. Mukhamedzhanov, Phys. Rev. A **47**, 2004 (1993).
[66] A. M. Mukhamedzhanov, A. S. Kadyrov, and F. Pirlepesov, Phys. Rev. A **73**, 012713 (2006).
[67] A. S. Kadyrov, I. Bray, A. M. Mukhamedzhanov, and A. T. Stelbovics, Ann. Phys. **324**, 1516 (2009).
[68] Since we work with the full interaction potential, the transition probability amplitudes include the heavy particle interaction, see Eq. (6).
[69] D. R. Bates and G. W. Griffing, Proc. Phys. Soc. (London) **67**, 663 (1954).
[70] We note in passing that calculation of polarisation parameter A_{20} may require even larger $b_{\max}$ [23].
[71] A. C. Laforge, K. N. Egodapitiya, J. S. Alexander, A. Hasan, M. F. Ciappina, M. A. Khakoo, and M. Schulz, Phys. Rev. Lett. **103**, 053201 (2009).
[72] H. Knudsen, U. Mikkelsen, K. Paludan, K. Kirsebom, S. P. Møller, E. Uggerhøj, J. Slevin, M. Charlton, and E. Morenzoni, Phys. Rev. Lett. **74**, 4627 (1995).